Nanoscale

ROYAL SOCIETY OF CHEMISTRY

COMMUNICATION

View Article Online
View Journal | View Issue

Cite this: *Nanoscale*, 2022, **14**, 3013

Received 29th January 2022,
Accepted 7th February 2022

DOI: 10.1039/d2nr00558a

rsc.li/nanoscale

Light-harvesting antennae based on copper indium sulfide (CIS) quantum dots†

Giacomo Morselli, [a] Alessandro Gradone,[a,b] Vittorio Morandi [b] and Paola Ceroni *[a]

Copper indium sulfide quantum dots (CIS QDs) and their core–shell analogues (CIS@ZnS QDs) were functionalized with pyrene chromophores *via* a dihydrolipoamide bifunctional binding moiety: UV excitation of the pyrene chromophores resulted in sensitized emission of the CIS core because of an efficient energy transfer process; the core–shell hybrid system exhibits a 50% increased brightness when excited at 345 nm.

Introduction

Copper indium sulfide quantum dots (**CIS QDs**) are a valid alternative to conventional quantum dots based on cadmium or lead due to their non-toxicity and good optical properties. Indeed, **CIS QDs** exhibit high molar absorption coefficients over the entire visible spectral region (10^4–10^5 M^{-1} cm^{-1}), elevated photoluminescence quantum yields (up to 70%) and long emission lifetimes (hundreds of nanoseconds).[1–3] The quantum dot properties can be varied by functionalizing its surface with molecules that can provide new features, *e.g.* colloidal stability in a different solvent. For **CIS QDs** this functionalization can be performed *via* ligand exchange, therefore substituting the original capping molecules used to stabilize the nanoparticle during its synthesis with other ones possessing an appropriate anchoring group, namely thiols.[4] By this approach, fluorophores can be conveniently used for the functionalization of **CIS QDs** to ameliorate the optical properties of the nanoparticle. In this context, nanoparticles can be decorated with a large number of chromophores that efficiently absorb the incoming light and then channel it to the quantum dot, which can emit at higher wavelengths, as assessed by our previous results on silicon quantum dots.[5–9] Such systems are called *light-harvesting antennae.*[10] More in general, light-harvesting antennae are organized multi-component systems in which many suitably organized chromophores absorb the incident light and then channel the excitation energy to a common acceptor component.[10] Many examples of such systems are also reported in nature, *e.g.* the green plant antenna system, where the light is absorbed by chlorophylls and the energy funnelled in the reaction center. In the case of emissive structures, light-harvesting antennae are characterized by a superior *brightness*‡ if compared to the isolated chromophores. This approach is rather unexplored in the case of **CIS QDs**. The only example we found in the literature is that of a mixture of core–shell **CIS@ZnS QDs** with an organic fluorophore (POPOP) acting as white-light-emitting (WLE) hybrid composite: the authors evidenced a possible energy transfer from the fluorophore to the nanoparticles with limited efficiency (<30%).[11]

In the present work, we describe the functionalization of **CIS QDs** with a ligand containing a UV-absorbing chromophore, namely pyrene. The ligand possesses a dihydrolipoamide moiety, therefore two thiol anchoring moieties that allow an efficient replacement of the original single thiol-containing ligand.[4] It is worth noting that dihydrolipoic acid derivatives have been widely used for the functionalization of cadmium-containing quantum dots,[12–17] but some examples are also reported for CIS-based nanoparticles.[18–20] The pyrene-functionalized nanoparticles are characterized by a superior absorption below 350 nm and a sensitized emission of the CIS QD upon pyrene excitation due to energy transfer from the organic chromophore towards the quantum dot. This represents the first example of a light-harvesting antenna based on copper indium sulfide quantum dots with enhanced brightness compared to the pristine sample without pyrene chromophores at the surface.

Results and discussion

Synthesis

Copper indium sulfide (CIS) QDs with or without a ZnS shell (hereafter named **CIS@ZnS QDs** and **CIS QDs**, respectively)

[a]*Department of Chemistry Ciamician, University of Bologna, Via Selmi 2, 40126 Bologna, Italy. E-mail: paola.ceroni@unibo.it*
[b]*CNR-IMM Bologna Section, Via Piero Gobetti 101, 40129 Bologna, Italy*

†Electronic supplementary information (ESI) available. See DOI: 10.1039/d2nr00558a

were synthesized according to a heating-up procedure adapted from literature.[21] The produced nanoparticles were stabilized and coated with an organic shell composed of 1-octanethiol, which allows a good dispersibility in non-polar solvents like chloroform. Afterwards, a partial ligand exchange with 6,8-dimercapto-*N*-(pyren-1-ylmethyl)octanamide (compound **2**) was performed. This molecule was chosen since it contains a dihydrolipoic acid-derivative moiety and therefore possesses two thiol groups that reinforce the interaction with the surface of the nanoparticle and therefore allows a more efficient replacement with the native mono-thiol ligand.[4] This was obtained firstly by amide coupling between lipoic acid and 1-pyrenemethylamine, followed by reduction of the sulfur–sulfur bond. The overall synthetical procedure is represented in Fig. 1. Ligand exchange was accomplished on both shelled and pristine quantum dots, yielding the samples named **CIS@ZnS-py QDs** and **CIS-py QDs**, respectively.

Structural and morphological characterization

The STEM-HAADF image of the sample **CIS@ZnS QDs** are reported in Fig. 2a. The distribution of the particles dimension is quite heterogenous with values from 2.5 nm up to 4 nm. The morphological characterization shows a triangular shape, particularly evident for some of the nanoparticles (see *e.g.*, the one indicated by the red arrow in Fig. 2a), consistent with the tetrahedral shape previously reported in literature.[21] The chalcopyrite crystalline phase was determined by Selected Area Electron Diffraction (SAED) indexing (Fig. 2b). The table in Fig. 2b displays all the measured *d*-spacings and the typical *d*-spacings of a chalcopyrite phase ($CuInS_2$). High resolution

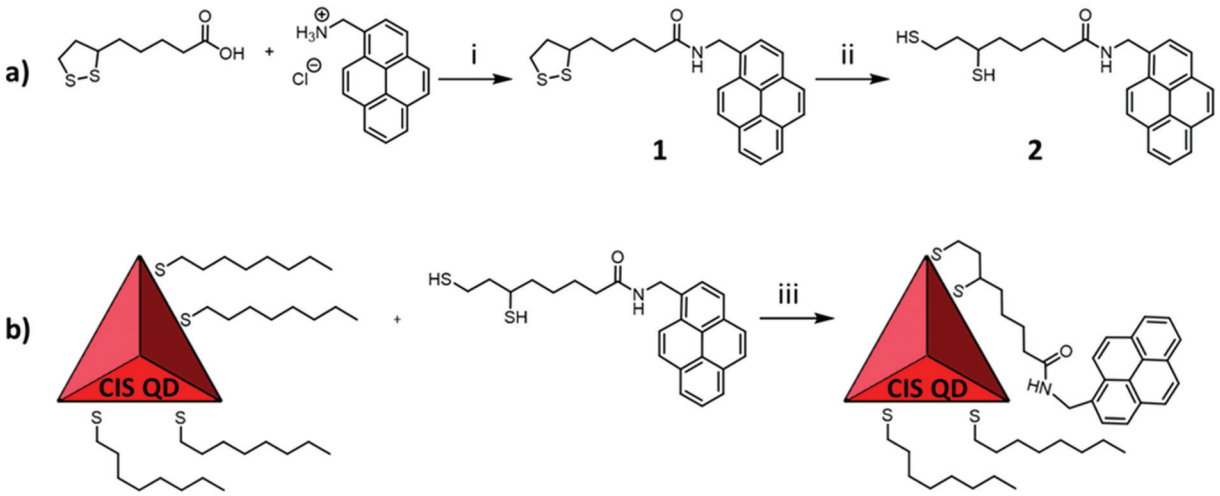

Fig. 1 Schematic representation of the adopted strategy to functionalize copper indium sulfide QDs with pyrene. (a) The synthesis of the ligand involves firstly an amide coupling between (±)-α-lipoic acid and 1-pyrenemethylamine hydrochloride, yielding compound **1**, followed by the reduction of the S–S bond, producing compound **2** (reaction conditions: i – HBTU, EDC, DIPEA, in DMF, 1 day; ii – $NaBH_4$ in DMF/water, 4 hours). (b) Ligand exchange to 1-octanethiol passivated **CIS QDs** or **CIS@ZnS QDs** (iii – chloroform, overnight) For simplicity purposes, few ligands per nanocrystal have been drawn.

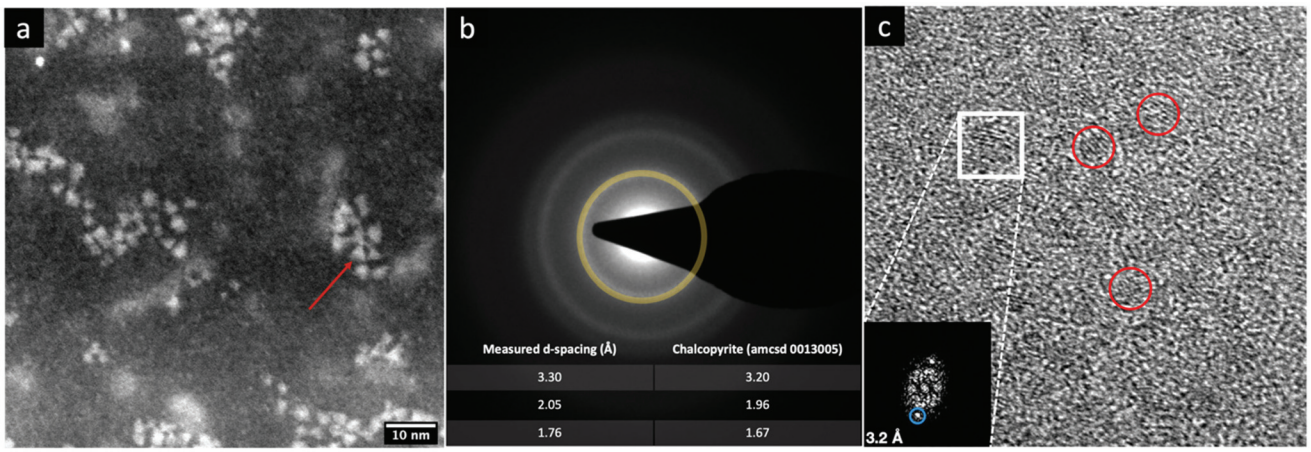

Fig. 2 (a) High magnification STEM micrographs, selected area electron diffraction (SAED) and (c) high resolution (HR) TEM image of **CIS@ZnS QDs**. The FFT (fast Fourier transform) in the inset refers to the zone highlighted with the white square.

micrograph (Fig. 2c) confirms the crystalline character of the nanoparticles (indicated by the red circles). The lattice spacing of 0.32 nm reported in the FFT inset (relative to the particle in the white square in Fig. 2c) is compatible with a tetragonal chalcopyrite phase. The same analyses were performed on the shell-free sample and are reported in Fig. S1a and S1b of the ESI.†

^{1}H-NMR spectroscopy was used to verify the presence of pyrene attached onto **CIS QDs** surface. Fig. 3 shows the overlap between the spectrum of compound **1** (green line) and **CIS@ZnS-py QDs** (red line) in $CDCl_3$. The main peaks are highlighted and associated to the protons of the molecule represented in the inset. The chemical shifts of the aromatic protons occur at around 7.7–8.3 ppm; signals at 3.0–3.5 ppm are due to the hydrogens in alpha position with respect to the sulfur atoms, at 2.0–2.2 ppm the band related to the protons linked to the carbon in proximity of the carboxylic group, while at about 1.2–1.4 ppm, the signals of the alkyl thiol chain are predominant, indication of a non-complete replacement of the native ligand. It is worth noting that the signals related to the hydrogens of the ligand attached to the quantum dot appear broadened due to the restricted motions that cause an enhancement of the relaxation times, as we also observed in previous works.[5,6] For comparison purposes, the NMR spectrum of the physical mixture compound **2** – **CIS@ZnS QDs** is reported in the ESI (Fig. S2†).

Photophysical properties

The absorption spectra of all the investigated sample of **CIS QDs** (Fig. 4) show the characteristic shoulder at *ca.*530 nm, which corresponds to the band gap transition. To better determine the corresponding wavelength, the local minimum of the second derivative of the spectra in the range 400–600 nm was evaluated, according to a procedure reported in literature (see Fig. S3 and S4 of the ESI† for further details).[22] In every case, the electronic transition occurs at 530 nm, corresponding to an energy gap of about 2.3 eV.

In the case of the pyrene-functionalized samples (blue lines), the typical absorption features of **CIS QDs** are overlapped to those of pyrene, clearly visible at 300–350 nm (black dashed lines). Since each component maintains its own absorption properties, no significant interaction occurs between the organic chromophore and the inorganic nanoparticle in the ground-state.

The average number of chromophores per nanocrystal can be estimated from the absorption spectra and the molar absorption coefficients (ε) of the present species. The molar absorption coefficient of the pyrene-based ligand is 4×10^4 M^{-1} cm^{-1} at 345 nm. For **CIS QDs**, we relied on the work from Booth *et al.*[22] who correlated the photophysical properties of copper indium sulfide quantum dots to their size. From their formula, it was possible to estimate the diameter of the CIS

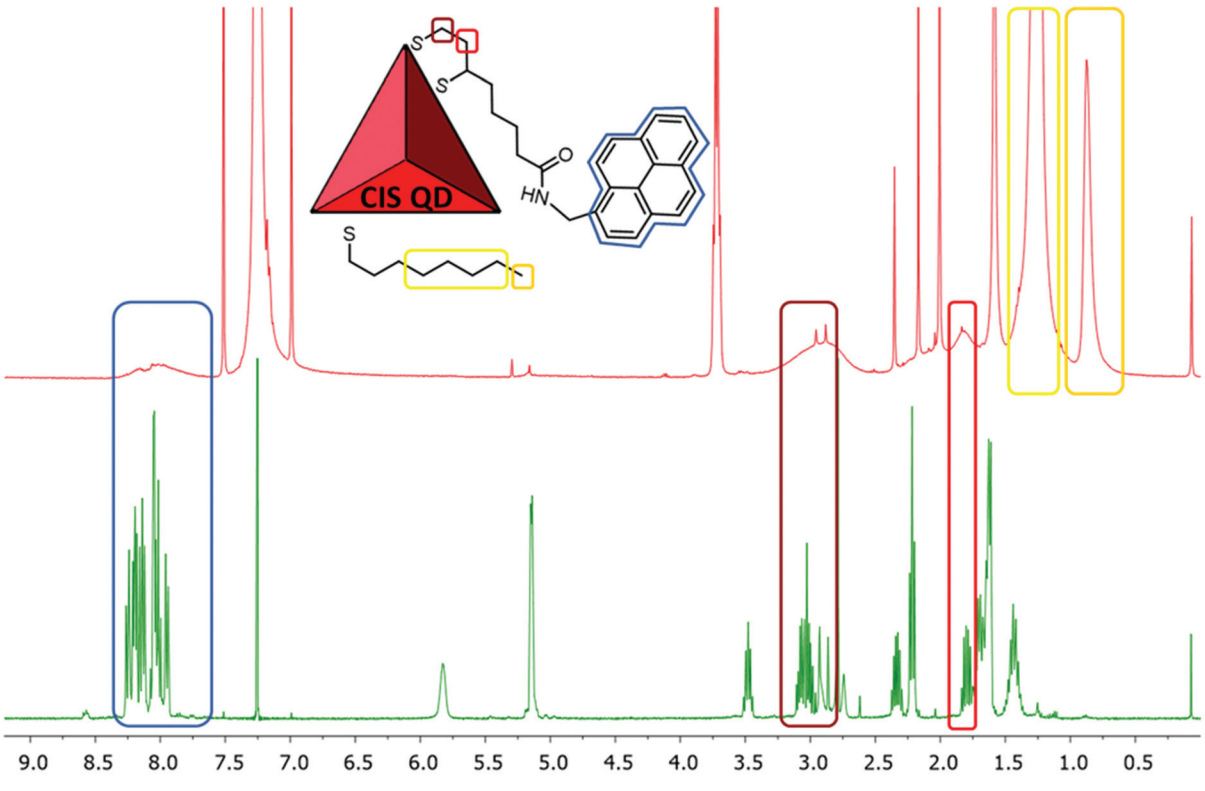

Fig. 3 ^{1}H-NMR (400 MHz, $CDCl_3$) spectra of compound **1** (green line) and **CIS@ZnS-py** (red line), which is schematized in the inset. The principal signals are highlighted to show the broadening of the peaks related to the attached molecules.

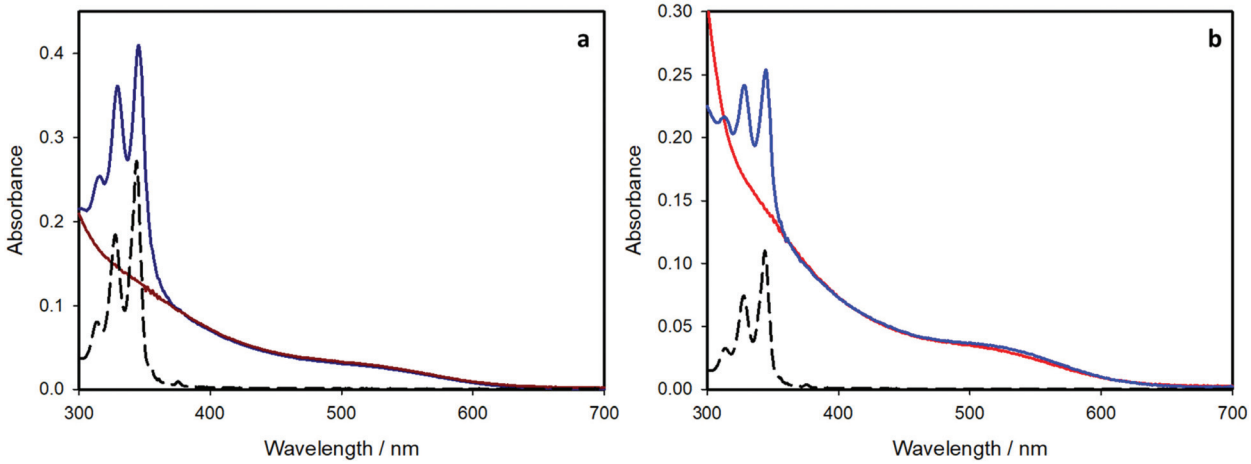

Fig. 4 Absorption spectra of (a) **CIS QDs** (dark red line) and **CIS-py QDs** (dark blue line) and (b) **CIS@ZnS QDs** (red line) and **CIS@ZnS-py QDs** (blue line) in chloroform, compared to the absorption spectrum of pyrene (black dashed line).

core for the samples, which is 3.6 nm and 2.7 nm for the shell-free and the ZnS-coated samples, respectively,§ which is in good accordance with the data obtained by TEM analysis. Moreover, the molar absorption coefficient computed at 530 nm (*i.e.* the first electronic transition), using the formula reported, is:

$$\varepsilon(530\ \text{nm}) = 830 \times d^{3.7}$$

where d is the diameter in nanometers and the result is expressed in $M^{-1}\ cm^{-1}$. Consequently, at 530 nm, where pyrene does not absorb, the molar absorption coefficients for **CIS QDs** and **CIS@ZnS QDs** are $9.5 \times 10^4\ M^{-1}\ cm^{-1}$ and $3.3 \times 10^4\ M^{-1}\ cm^{-1}$, respectively. From these data the average number of pyrene moieties per nanocrystals is estimated to be about 20 for **CIS-py QDs** and 3 for **CIS@ZnS-py QDs**.¶ In our opinion, this discrepancy can be due to a different surface reactivity towards the dihydrolipoamide either because of the different composition exposed ($CuInS_2$ or ZnS), or because of the different dimensions of the nanoparticles.[23]

Upon selective excitation of the nanocrystal core at 450 nm, the emission spectrum features a bell-shaped band centered at 710 nm for the shell-free quantum dots and 650 nm for the ZnS-coated ones (Fig. 5 and Table 1). This blue-shift is well-known for such core–shell QDs and is associated to an inter-diffusion of zinc ions into the CIS core[24] and an etching of the core material.[21] As expected,[1,2,21] the emission quantum yield remarkably increases upon coating the nanocrystals with a ZnS shell.

If we now consider the effect of ligand exchange on the emission quantum yield upon selective excitation of the nanocrystal at 450 nm, two opposite behaviors are observed. For the pristine nanoparticles, the emission quantum yield decreases

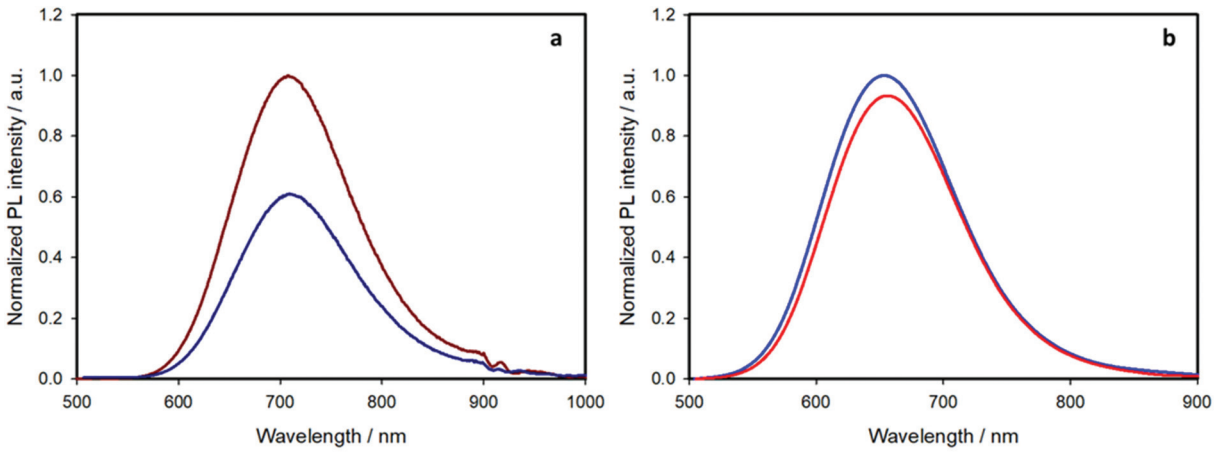

Fig. 5 Emission spectra with intensity proportional to the corresponding emission quantum yields of (a) **CIS QDs** (dark red line) and **CIS-py QDs** (dark blue line) and (b) **CIS@ZnS QDs** (red line) and **CIS@ZnS-py QDs** (blue line) in chloroform; λ_{ex} = 450 nm. The relative intensities in each panel reflect the corresponding emission quantum yields.

Table 1 Main photophysical properties of the studied quantum dots in air-equilibrated chloroform suspension

	Pyrene emission		Quantum dot emission		
	λ_{em} (nm)	τ^a (ns)	λ_{em} (nm)	τ^b (ns)	PLQY^c (%)
CIS QDs	—	—	710	70	1.9
CIS-py QDs	395	1.4 (0.08) 20 (0.02)	710	50	1.2
CIS@ZnS QDs	—	—	650	350	28
CIS@ZnS-py QDs	395	1.0 (0.04) 20 (0.01)	650	260	30

[a] Excitation at 340 nm, emission at 390 nm (pre-exponential factor between brackets). [b] Weighted average lifetime, excitation at 405 nm, emission at the corresponding maximum. [c] Excitation at 450 nm.

(from 1.9% to 1.2%, Table 1), a phenomenon associated to the introduction of surface defects.[1,25,26] On the other hand, the quantum yield of the shelled sample slightly increased (from 28% to 30%, Table 1).

Exciting at 345 nm, where the 44% and 68% of light is also absorbed by pyrene, for the core–shell and the shell-free samples, respectively, the emission spectra feature two additional bands (Fig. 6): a structured band with maximum at 395 nm, due to the emission of pyrene monomer, and a broad band peaked at 480 nm, correlated to the emission of pyrene excimer (characterized by a lifetime of 30 ns). For a solution of free pyrene chromophores, excimer emission is observed only at concentration higher than 10^{-4} M.[27] In the present case, the sample concentration is lower than 5×10^{-5} M and the presence of excimer is related to pyrene close proximity at the nanocrystal surface, as also reported for other pyrene-functionalized quantum dots.[6,28]

The pyrene monomer emission at 395 nm is strongly quenched for both samples. This is confirmed by the lifetime measurements reported in Table 1. For both pyrene-containing samples, the emission decay at 395 nm (upon excitation at 340 nm) can be fitted by a bi-exponential function: the shorter component (*ca.* 1 ns) corresponds to the quenched pyrene chromophores attached at the nanocrystal surface and the long component (20 ns) is equal to that of the free pyrene ligand (compound **2** in air-equilibrated chloroform). The quenching efficiency is *ca.* 95% for both the samples. The kinetic rate constants for the quenching process are 6.6×10^8 s^{-1} and 9.5×10^8 s^{-1} for the shell-free and the core–shell system, respectively, as estimated by the comparison of the emission lifetimes (see ESI† for more details).

The presence of free pyrene ligand is expected: the binding of the ligand at the nanocrystal surface is dynamic, as previously reported for typical quantum dots,[29–33] and an equilibrium between free and attached chromophores is contemplated. From the pre-exponential factors of the two lifetimes, we can estimate that the free pyrene ligand is around 20% for both samples (see ESI† for more details).

The above-discussed quenching process of the pyrene emission is related to energy transfer from the pyrene chromophore to the CIS core, as demonstrated by the excitation spectra performed at an emission wavelength of 700 nm. Fig. 7 displays the excitation spectra of the pyrene-functionalized samples (blue lines) compared to the chromophore-free samples (red lines) and their absorption spectra (green lines).

The pyrene-functionalized samples show the characteristic pyrene absorption peaks in the range 300–350 nm, demonstrating that the emission of the inner CIS QD is sensitized by pyrene: excitation of the organic chromophore at wavelengths lower than 350 nm results in an energy transfer to the nanoparticle, which emits at *ca.* 700 nm (a schematic representation of the energy level diagram and the energy transfer process is reported in Fig. S5†). This is, to the best of our knowledge, the first case of an efficient light-harvesting antenna based on copper indium sulfide quantum dots.

The brightness of the shell-free sample did not receive benefits by the enhanced absorption, because of the concomitant strong decrease of the intrinsic emission quantum yield

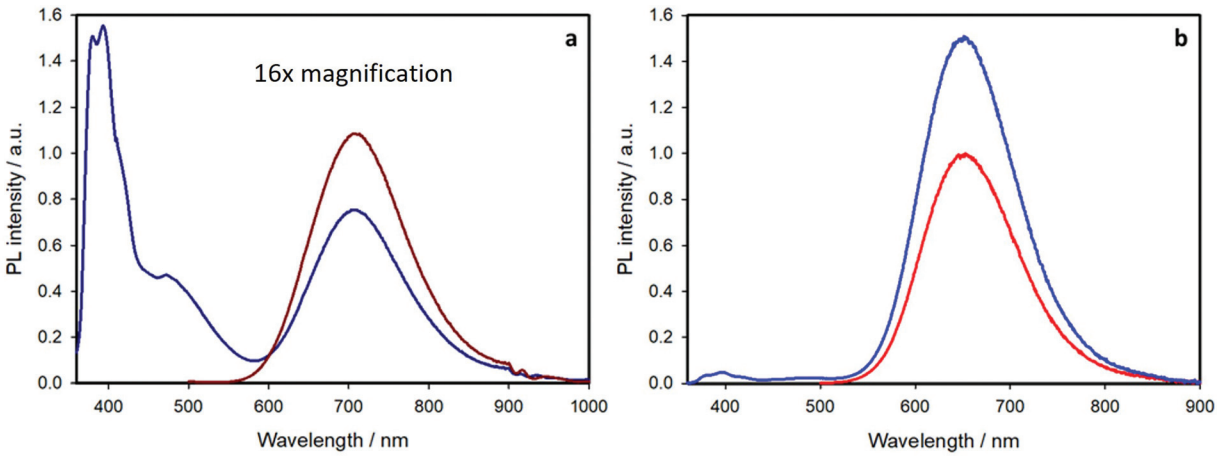

Fig. 6 Emission spectra of equimolar suspensions of (a) **CIS QDs** (dark red line) and **CIS-py QDs** (dark blue line) and (b) **CIS@ZnS QDs** (red line) and **CIS@ZnS-py QDs** (blue line) in chloroform, exciting at 345 nm. The emission spectra in (a) are magnified by a 16 factor for comparison purposes.

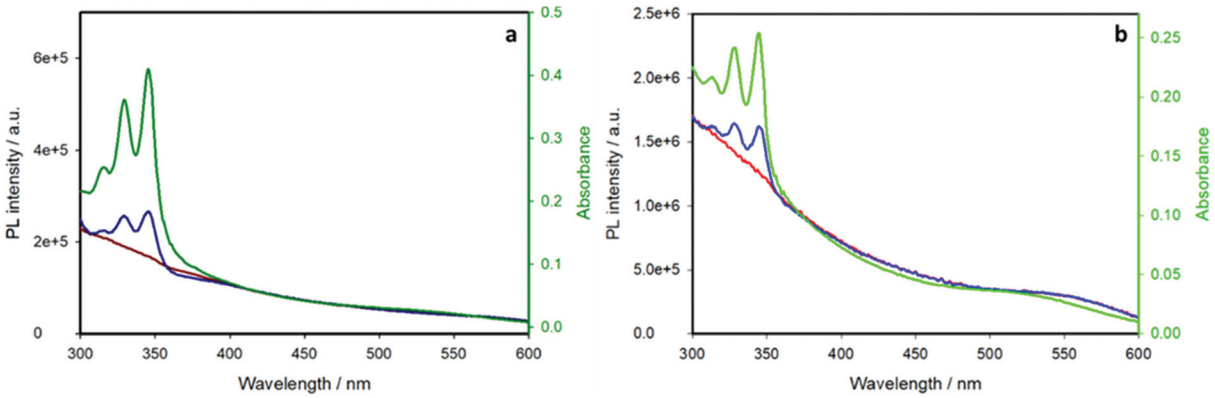

Fig. 7 Excitation spectra of (a) **CIS QDs** (dark red line) and **CIS-py QDs** (dark blue line) compared to the absorption spectrum of **CIS-py QDs** (green line) and (b) **CIS@ZnS QDs** (red line) and **CIS@ZnS-py QDs** (blue line) with the absorption profile of **CIS@ZnS-py QDs** in chloroform. λ_{em} = 700 nm.

of the nanoparticle upon ligand exchange, as previously discussed. On the contrary, for the core–shell sample, the brightness (relative to the emission at 700 nm upon excitation at 345 nm) increases of 50% for **CIS@ZnS-py QDs** compared to **CIS@ZnS QDs**. This result highlights the importance of coating the quantum dot with a ZnS layer to optimize their luminescence performance.

It is interesting to notice that **CIS@ZnS QDs** enhance their emissive properties after ligand exchange: most of the literature examples report an opposite trend because ligand exchange causes the introduction of defective states.[34] In our opinion, this was possible due to (i) a partial exchange of the native alkyl thiol ligands, (ii) the linkage with an efficient chromophore and (iii) the presence of a protective ZnS shell.

The introduction of a higher amount of pyrene chromophore was also attempted: the reaction with a 4-times higher concentration of compound **2** yielded **CIS@ZnS QDs** functionalized with 13 pyrene units, demonstrating that the amount of the linked chromophore can be tuned on purpose. However, the signal of the pyrene excimer emission was predominant, due to the high amount of chromophore. Therefore, also the energy transfer efficiency was compromised (see ESI and Fig. S6† for more details).

Conclusions

We have successfully functionalized copper indium sulfide quantum dots and their core–shell analogues, namely **CIS@ZnS QDs**, with a dihydrolipoamide derivative bearing a pyrene moiety. The resulting systems act as light-harvesting antennae: pyrene increases the absorption properties and sensitizes the emission of the quantum dot at 700 nm. In particular, for the ZnS coated sample, we observed a substantial improvement of the photoluminescence properties of the quantum dot, with an increase of the brightness up to 50% when exciting at 345 nm. We believe that this is particularly advantageous for water-suspendable systems, since PLQY of quantum dots usually decreases when transferred in polar solvents.[1,12,26] The enhanced absorption, along with the energy transfer process to the quantum dot can compensate this effect.

Functionalization with chromophores absorbing in the visible range and with a more stable binding are ongoing in our laboratories.

Conflicts of interest

There are no conflicts to declare.

Acknowledgements

The University of Bologna is gratefully acknowledged for financial support. The European Union's Horizon 2020 Research and Innovation Program (Grant Agreement No. 881603 Graphene Flagship Core Project 3, and Grant Agreement No. 861857 "CHALLENGES" project) is acknowledged.

Notes and references

‡ Brightness is defined as the product between the molar absorption coefficient at the excitation wavelength and the sensitized emission quantum yield of the system.

§ The formula used to compute the diameter core d from the emission maximum wavelength λ in nm is: $d = 68.952 - 0.2136\,\lambda + 1.717 \times 10^{-4}\,\lambda^2$.

¶ The reported values have been corrected for the pyrene chromophores not attached at the nanocrystal surface, as evaluated by the analysis of emission lifetimes.

1 A. D. P. Leach and J. E. Macdonald, *J. Phys. Chem. Lett.*, 2016, **7**, 572–583.
2 H. Zhong, Z. Bai and B. Zou, *J. Phys. Chem. Lett.*, 2012, **3**, 3167–3175.
3 G. Morselli, M. Villa, A. Fermi, K. Critchley and P. Ceroni, *Nanoscale Horiz.*, 2021, **6**, 676–695.
4 J. Kolny-Olesiak and H. Weller, *ACS Appl. Mater. Interfaces*, 2013, **5**, 12221–12237.

5 R. Mazzaro, A. Gradone, S. Angeloni, G. Morselli, P. G. Cozzi, F. Romano, A. Vomiero and P. Ceroni, *ACS Photonics*, 2019, **6**, 2303–2311.
6 G. Morselli, F. Romano and P. Ceroni, *Faraday Discuss.*, 2020, **222**, 108–121.
7 M. Locritani, Y. Yu, G. Bergamini, M. Baroncini, J. K. Molloy, B. A. Korgel and P. Ceroni, *J. Phys. Chem. Lett.*, 2014, **5**, 3325–3329.
8 A. Fermi, M. Locritani, D. Carlo, M. Pizzotti, S. Caramori, Y. Yu, B. A. Korgel and P. Ceroni, *Faraday Discuss.*, 2015, **185**, 481–495.
9 L. Ravotto, Q. Chen, Y. Ma, S. A. Vinogradov, M. Locritani, G. Bergamini, F. Negri, Y. Yu, B. A. Korgel and P. Ceroni, *Chem*, 2017, **2**, 550–560.
10 F. Romano, Y. Yu, B. A. Korgel, G. Bergamini and P. Ceroni, *Top. Curr. Chem.*, 2016, **374**, 89–106.
11 P. Ilaiyaraja, P. S. V. Mocherla, T. K. Srinivasan and C. Sudakar, *ACS Appl. Mater. Interfaces*, 2016, **8**, 12456–12465.
12 H. T. Uyeda, I. L. Medintz, J. K. Jaiswal, S. M. Simon and H. Mattoussi, *J. Am. Chem. Soc.*, 2005, **127**, 3870–3878.
13 N. Zhan, G. Palui, M. Safi, X. Ji and H. Mattoussi, *J. Am. Chem. Soc.*, 2013, **135**, 13786–13795.
14 G. Palui, T. Avellini, N. Zhan, F. Pan, D. Gray, I. Alabugin and H. Mattoussi, *J. Am. Chem. Soc.*, 2012, **134**, 16370–16378.
15 K. Susumu, T. Pons, I. L. Medintz and H. Mattoussi, *Mater. Res. Soc. Symp. Proc.*, 2007, **1019**, 76–81.
16 J. Park, J. Nam, N. Won, H. Jin, S. Jung, S. Jung, S. H. Cho and S. Kim, *Adv. Funct. Mater.*, 2011, **21**, 1558–1566.
17 J. Zhou, Y. Liu, J. Tang and W. Tang, *Mater. Today*, 2017, **20**, 360–376.
18 J. Feng, M. Sun, F. Yang and X. Yang, *Chem. Commun.*, 2011, **47**, 6422–6424.
19 L. Li, T. J. T. Daou, I. Texier, T. K. Chi, T. T. Kim Chi, N. Q. Liem and P. Reiss, *Chem. Mater.*, 2009, **21**, 2422–2429.
20 T. Pons, E. Pic, N. Lequeux, E. Cassette, L. Bezdetnaya, F. Guillemin, F. Marchal and B. Dubertret, *ACS Nano*, 2010, **4**, 2531–2538.
21 L. Li, A. Pandey, D. J. Werder, B. P. Khanal, J. M. Pietryga and V. I. Klimov, *J. Am. Chem. Soc.*, 2011, **133**, 1176–1179.
22 M. Booth, A. P. Brown, S. D. Evans and K. Critchley, *Chem. Mater.*, 2012, **24**, 2064–2070.
23 L. Liu, X. Zhang, L. Ji, H. Li, H. Yu, F. Xu, J. Hu, D. Yang and A. Dong, *RSC Adv.*, 2015, **5**, 90570–90577.
24 J. Park and S. W. Kim, *J. Mater. Chem.*, 2011, **21**, 3745–3750.
25 M. Booth, R. Peel, R. Partanen, N. Hondow, V. Vasilca, L. J. C. Jeuken and K. Critchley, *RSC Adv.*, 2013, **3**, 20559–20566.
26 N. Tsolekile, S. Parani and M. C. Matoetoe, *Nano-Struct. Nano-Objects*, 2017, **12**, 46–56.
27 V. Balzani, P. Ceroni and A. Juris, *Photochemistry and Photophysics - Concepts, Research, Applications*, Wiley-VCH, 1 edn, 2015.
28 R. Mazzaro, M. Locritani, J. K. Molloy, M. Montalti, Y. Yu, B. A. Korgel, G. Bergamini, V. Morandi and P. Ceroni, *Chem. Mater.*, 2015, **27**, 4390–4397.
29 S. Silvi and A. Credi, *Chem. Soc. Rev.*, 2015, **44**, 4275–4289.
30 M. Green, *J. Mater. Chem.*, 2010, **20**, 5797–5809.
31 A. Loiudice, O. Segura Lecina, A. Bornet, J. M. Luther and R. Buonsanti, *J. Am. Chem. Soc.*, 2021, **143**, 13418–13427.
32 R. R. Knauf, J. C. Lennox and J. L. Dempsey, *Chem. Mater.*, 2016, **28**, 4762–4770.
33 W. Liu, A. B. Greytak, J. Lee, C. R. Wong, J. Park, L. F. Marshall, W. Jiang, P. N. Curtin, A. Y. Ting, D. G. Nocera, D. Fukumura, R. K. Jain and M. G. Bawendi, *J. Am. Chem. Soc.*, 2010, **132**, 472–483.
34 Z. Long, W. Zhang, J. Tian, G. Chen, Y. Liu and R. Liu, *Inorg. Chem. Front.*, 2021, **8**, 880–897.